Efficient Multi-floor Indoor Mapping with A Versatile Rotating LiDAR System

Yangzi Cong [1,2,3], Tianhe Xu [2], Chi Chen [3], Wenfeng Nie [2], Bisheng Yang[3]

[1] Key Laboratory of Smart Earth, Beijing, China – yzcong@sdu.edu.cn
[2] School of Space Science and Physics, Shandong University, Weihai, Shandong, China - thxu@sdu.edu.cn, wenfengnie@sdu.edu.cn
[3] State Key Laboratory of Information Engineering in Surveying, Mapping and Remote Sensing, Wuhan University, Wuhan, China – chichen@whu.edu.cn, bshyang@whu.edu.cn

Keywords: Indoor Mapping, Sensor Fusion, SLAM, Rotating LiDAR.

Abstract

Light Detection And Ranging (LiDAR) technology has provided an impactful way to capture 3D environmental map. However, consistent mapping in sensing-degenerated and perceptually-limited scenes (e.g. multi-story buildings) or under high dynamic sensor motion (e.g. rotating platform) remains a significant challenge. To this end, an efficient multi-floor indoor mapping system is proposed in this paper utilizing a versatile rotating LiDAR platform. In the front end, measurements from motor, IMU and LiDAR are tightly integrated to track the fast motion state of system, based on iterative Error State Kalman Filter (ESKF). Then linear and planar features are extracted from the point cloud map voxelized with adaptive resolutions. A sliding-window-based batch optimization is performed to simultaneously optimize the states of local frames with reference to the map consistency. In the experiments, we investigated the influence of rotating speed on the mapping performance as well as the superiority of rotating mechanism when compared to standard LiDAR setup. Moreover, comparative studies with one of the SOTA work, FAST-LIO2, have shown the competitive mapping results in multi-floor indoor environments.

1. Introduction

The urgency of 3D spatial mapping for digital twin modelling has been underscored in recent research (Lehtola et al., 2022). The development of mobile mapping systems, from sensors to applications, has garnered significant attention, promising precise and robust 3D reconstruction (Elhashash et al., 2022). In addition to the widespread use of GNSS for large-scale outdoor scenes, the field of Simultaneous Localization And Mapping (SLAM) has consistently emphasized the complex task of 3D mapping in extreme underground or confined indoor environments with intricate self-similar structures (Ebadi et al., 2022). LiDAR stands out as a crucial sensor for accurate pose estimation, laying a solid foundation for acquiring high-precision point cloud maps. Compared to other sensors, LiDAR offers high measurement accuracy, rapid response speed, and strong anti-interference capabilities.

Due to the limited vertical angle resolution (e.g., 2 degrees) of Multi-Beam LiDAR (MBL) compared to its horizontal resolution (e.g., 0.2 degrees), there is typically varying degrees of drift in the height/Z direction of the estimated trajectory (Liu et al., 2019; Seo et al., 2022; Wei et al., 2021). To mitigate this drift, numerous studies utilize the ground as a strong constraint (Chen et al., 2021; Koide et al., 2019; Seo et al., 2022; Shan and Englot, 2018; Velas et al., 2019; Wei et al., 2021), while others introduce additional vertical residuals in LiDAR SLAM (Zelin Wang et al., 2022). Moreover, some researchers extract various types of features, including ground, facade, pillar, and beam, to enhance pose estimation robustness (Pan et al., 2021; Zhou et al., 2021). By adaptively filtering and probabilistically modeling the local point cloud map, efforts have been made to enhance the accuracy of LiDAR odometry (LO) and the mapping process (Duan et al., 2022; Garcia-Fidalgo et al., 2022; Quenzel and Behnke, 2021; Yuan et al., 2022). However, relying solely on LiDAR may not be sufficient to recover high dynamic motion states in a short period, and long-term LiDAR odometry could suffer from significant accumulated error. As a result, LiDAR-inertial-odometry (LIO) systems, which integrate LiDAR and IMU data either loosely or tightly, have been developed to provide rapid and accurate positioning across various scenarios (Bosse et al., 2012; Kenny Chen et al., 2022; Holmberg et al., 2022; Le Gentil et al., 2020; Qian et al., 2022; Zhong Wang et al., 2022). The high-frequency state measurements from IMUs aid in guiding LiDAR registration towards improved convergence, while the slowly varying biases of IMUs are concurrently estimated through the registration process.

To compensate the limited field of view (FoV) and resolution of a single laser scanner, researchers have explored 3D mapping using multiple LiDARs as discussed in (Chen et al., 2021; Jiao et al., 2021; Velas et al., 2019). These efforts aim not only to improve pose estimation but also to achieve comprehensive reconstruction of the environment. To achieve uniform observations in all directions, a pair of tilted-mounted laser scanners is employed. Building on the work of (Zhang and Singh, 2017), other studies have focused on enhancing mapping quality using a rotating 2D LiDAR (Alismail and Browning, 2015; Kang and Doh, 2016; Yuan et al., 2021; Zhen et al., 2017). These systems place the 2D LiDAR on a rotating platform to increase the field of view. The pioneering work of (Park et al., 2021, 2018, 2017) has led to the development of the first map-centric SLAM framework for dense elastic mapping of environments. Meanwhile, with the advancement of 3D LiDAR technology, researchers have carefully examined the effectiveness of Multi-Beam LiDAR (MBL) installed on a rotating platform (Claer et al., 2019; Morales et al., 2018; Neumann et al., 2016). In addition, Karimi et al. (2021) have investigated the relationship between scan patterns and rotation mechanisms to enhance SLAM performance. They propose a 2D Lissajous pattern to rotate the LiDAR for equitable observation of vertical and horizontal surfaces. Similarly, Ramezani et al.(2022) and Kai Chen et al. (2022) have developed commendable LiDAR-inertial-odometry (LIO) systems, although they devote less attention to the design of the rotating platform setup itself.

The integration of a rotating Multi-Beam LiDAR (MBL) with an Inertial Measurement Unit (IMU) is paramount for achieving robust 3D mapping under high dynamic motion, particularly in multi-story scenes. However, this integration poses two primary

challenges. Firstly, mounting the MBL on a motor introduces an additional sensor motion pattern alongside the body's movement. This combined motion state complicates accurate pose estimation. Secondly, the distribution characteristics of MBL point clouds vary over time due to rotation, necessitating additional efforts for robust point cloud registration, especially in narrow indoor scenes. To address these challenges, we introduce a novel LiDAR-inertial-mapping system designed for rotating MBL platforms for efficient multi-floor indoor mapping. In the front end, an Error State Kalman Filter (ESKF) is utilized in the LiDAR-inertial odometry (LIO) module to track fast motion states. Subsequently, to maintain the global map consistency, linear and planar voxels are extracted and expanded from the reconstructed point cloud map to establish associations among multiple frames in the sliding window. The experiments with various setting are carried out to exemplify the mapping performance of our system.

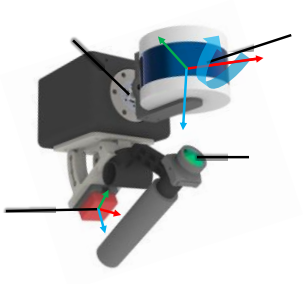

Figure 1. Mapping system design.

Sensor	Frequency/Hz	Parameters
LiDAR	10	Beams number: 16 Ranging accuracy: 3cm Horizontal angle resolution: 0.2° Vertical angle resolution: 2° FoV: 360°x30°
Motor	200	Angle accuracy: $^{1}/_{2^{16}}$ °
IMU	200	Accelerometer zero-bias stability: 15ug Gyroscope zero-bias stability: 3°/h

Table 1. Sensor specifications.

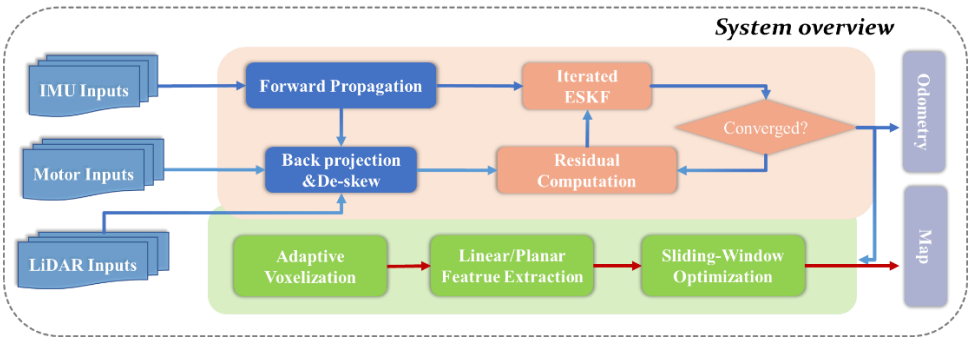

Figure 2. Mapping system overview

2. System Overview

Our versatile mapping system is shown in Figure 1 rigidly coupled with a handle. It consists of an electric motor ***M***, an attached Velodyne LiDAR ***L*** with sparse 16 laser beams, a built-in Xsens Mti-300 MEMS IMU ***I*** and a fisheye camera (for visualization only at present). Detailed specifications can be found in Table 1. The reason for not placing IMU right on the top of LiDAR lies on the consideration of stability for gyroscope and accelerator. The clock of each sensor is hard-synchronized through the signal from an ARM. The system overview is demonstrated in Figure 2 with different models explained in the following subsections.

2.1 Motor model

The LiDAR rotates around the X axis of body (IMU) frame producing different roll angles for laser points. The fixed extrinsic transformation between IMU and LiDAR is calibrated offline while the rotation angle for each point is compensated by the motor angle data output, the precision of which is $^{1}/_{2^{16}}$ in 200 Hz. In specific, this angle is linearly interpolated between the motor angles of the nearest two timestamps t_i^M, t_{i+1}^M with reference to the point timestamp t_i^L as shown in Figure 3

$$
\begin{aligned}
{}^{I}\boldsymbol{p}_{t_i^L} &= {}_{L}^{I}\boldsymbol{T} \cdot {}^{L}\boldsymbol{p}_{t_i^L} \\
&= {}_{L}^{I}\boldsymbol{T}_{calib} \cdot \mathbf{R}\left(t_i^L, t_i^M, t_{i+1}^M\right) {}^{L}\boldsymbol{p}_{t_i^L},
\end{aligned} \tag{1}
$$

Where $\mathbf{R}(*)$ is 3x3 rotation matrix only with roll angle. In this way, we can get each laser point in the frame of IMU.

2.2 IMU model

With IMU measurement model, we can incrementally propagate the system state forwardly at each IMU timestamp t_i^I. Thus, the motion distortion within the LiDAR scan will be rectified by projecting the laser points according to the time difference as shown in Figure 3. Detailed state propagation process and equation derivation can be found in the work of (Xu and Zhang, 2020).

$$
{}^{I}\boldsymbol{p}_{t_j^I} = {}_{t_i^L}^{t_j^I}\boldsymbol{T} \cdot {}^{I}\boldsymbol{p}_{t_i^L}, \tag{2}
$$

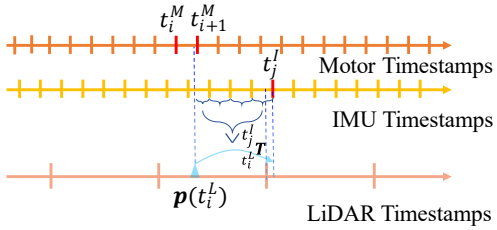

Figure 3. Multi-sensor temporal synchronization.

2.3 LiDAR model

The undistorted point clouds are then transformed to the world (map) frame $\boldsymbol{W}$ using

$$ {}^{W}\boldsymbol{p}_{t_j^I} = {}^{W}_{I}\boldsymbol{T} \cdot {}^{I}\boldsymbol{p}_{t_j^I}, \tag{3} $$

where five nearest neighbours are found to determine the local small surface. The residual will be defined by the point-to-surface distance. This optimization can be solved iteratively by ESKF method as detailed in (Xu and Zhang, 2020). However, there are abundant similar structures in multi-floor indoor environments causing such constraint function to degenerate. To enhance robustness, we calculate the average residuals after each optimization to filter out gross error.

2.4 Optimization model

From the above LIO process, the system states can be finely obtained at LiDAR frame frequency. However, global consistency cannot be guaranteed especially when mapping across multiple floors with a rotating MBL. Thus, we choose BALM (Liu and Zhang, 2021) as the back-end for sliding-window-based optimization. To begin with, local point cloud map is constructed and voxelized through the integration of downsampled LiDAR frames in the window. Then from octree roots with large-scale resolution to leaves with small-scale one, PCA analysis is conducted to extract linear and planar voxels by examination of eigenvalues. Suppose $\boldsymbol{n}$ is the normal of planar voxels or direction of linear voxels, ${}^{W}\boldsymbol{q}$ is one point on them. The target of bundle adjustment can be illustrated in Equation (4)(5), where the system states will be refined in accord with the map consistency. Followed BALM, we use second order approximation to minimize the different eigenvalues of feature covariance matrix Ω, by Levenberg-Marquardt (LM) method. Since each feature voxel consists of points from multiple frames, such batch optimization is conducted in a sliding window scheme, where the covariance of marginalized frames is kept fixed in the map voxel for efficiency. More implementation details can be found in (Liu and Zhang, 2021).

$$ \begin{aligned} (\boldsymbol{T}^*, \boldsymbol{n}^*, {}^{W}\boldsymbol{q}^*) &= \arg\min_{\boldsymbol{T},\boldsymbol{n},{}^{W}\boldsymbol{q}} \frac{1}{N}\sum_{i=1}^{N} \left(\boldsymbol{n}^T\left({}^{W}\boldsymbol{p}_i - {}^{W}\boldsymbol{q}\right)\right)^2 \\ &= \arg\min_{\boldsymbol{T}} \left\{ \min_{\boldsymbol{n},{}^{W}\boldsymbol{q}} \frac{1}{N}\sum_{i=1}^{N} \left(\boldsymbol{n}^T\left({}^{W}\boldsymbol{p}_i - {}^{W}\boldsymbol{q}\right)\right)^2 \right\} \overset{\text{def}}{=} \arg\min_{\boldsymbol{T}} \lambda_{min}(\Omega), \end{aligned} \tag{4} $$

$$ \begin{aligned} (\boldsymbol{T}^*, \boldsymbol{n}^*, {}^{W}\boldsymbol{q}^*) &= \arg\min_{\boldsymbol{T},\boldsymbol{n},{}^{W}\boldsymbol{q}} \frac{1}{N}\sum_{i=1}^{N} \left\|(\boldsymbol{I} - \boldsymbol{n}\boldsymbol{n}^T)\left({}^{W}\boldsymbol{p}_i - {}^{W}\boldsymbol{q}\right)\right\|_2^2 \\ &= \arg\min_{\boldsymbol{T}} \left\{ \min_{\boldsymbol{n},{}^{W}\boldsymbol{q}} \frac{1}{N}\sum_{i=1}^{N} \left\|(\boldsymbol{I} - \boldsymbol{n}\boldsymbol{n}^T)\left({}^{W}\boldsymbol{p}_i - {}^{W}\boldsymbol{q}\right)\right\|_2^2 \right\} \overset{\text{def}}{=} \arg\min_{\boldsymbol{T}} \left(Tr(\Omega) - \lambda_{max}(\Omega)\right), \end{aligned} \tag{5} $$

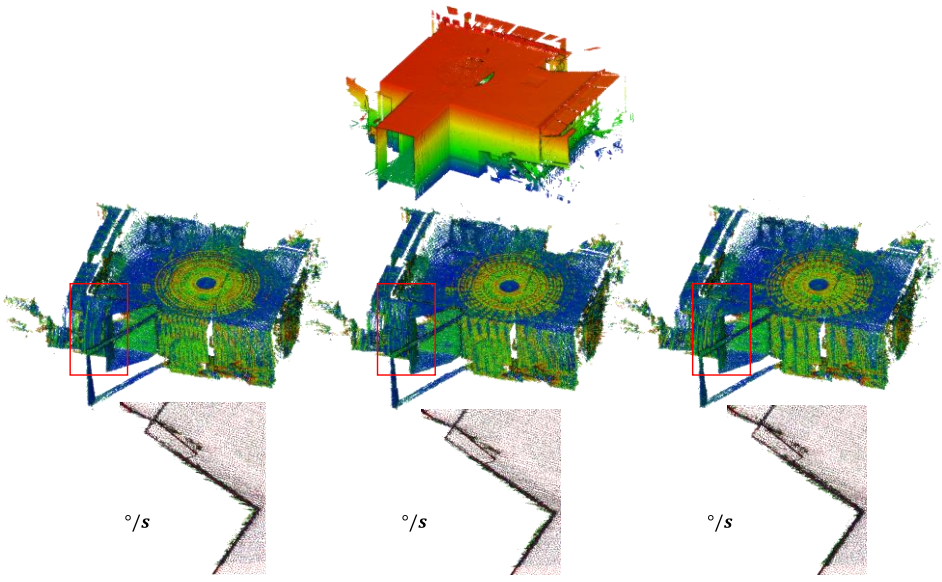

Figure 4. Mapping results of different rotating speeds.

3. Experimental Results

3.1 Influence of rotating speed

At first, to investigate the influence of motor rotating speed on the mapping performance, the system is fixed on the ground of

an office room where 5 minutes of data are collected and processed. Three different rotating speeds are tested for comparison with high-precision TLS map scanned by Leica VZ400 with a measuring accuracy of 3mm. The cloud-to-cloud distances are calculated through the *CloudCompare* software. From Figure 4, we can see $90°/s$ achieves the best precision with thinnest wall, which is in accord with most commercial handheld mapping device. So, we chose it as the baseline in the following experiments.

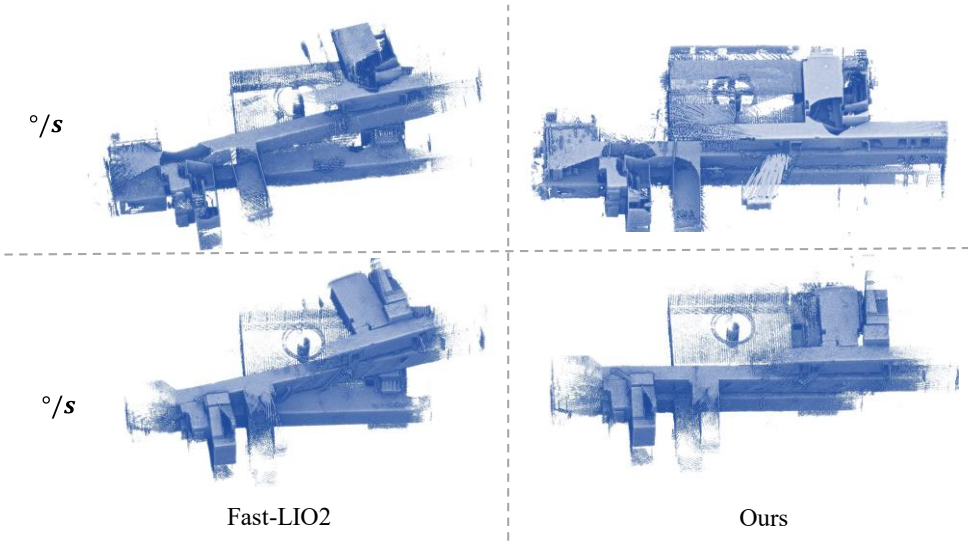

Figure 5. Multi-floor mapping results of different methods w\o rotating mechanism.

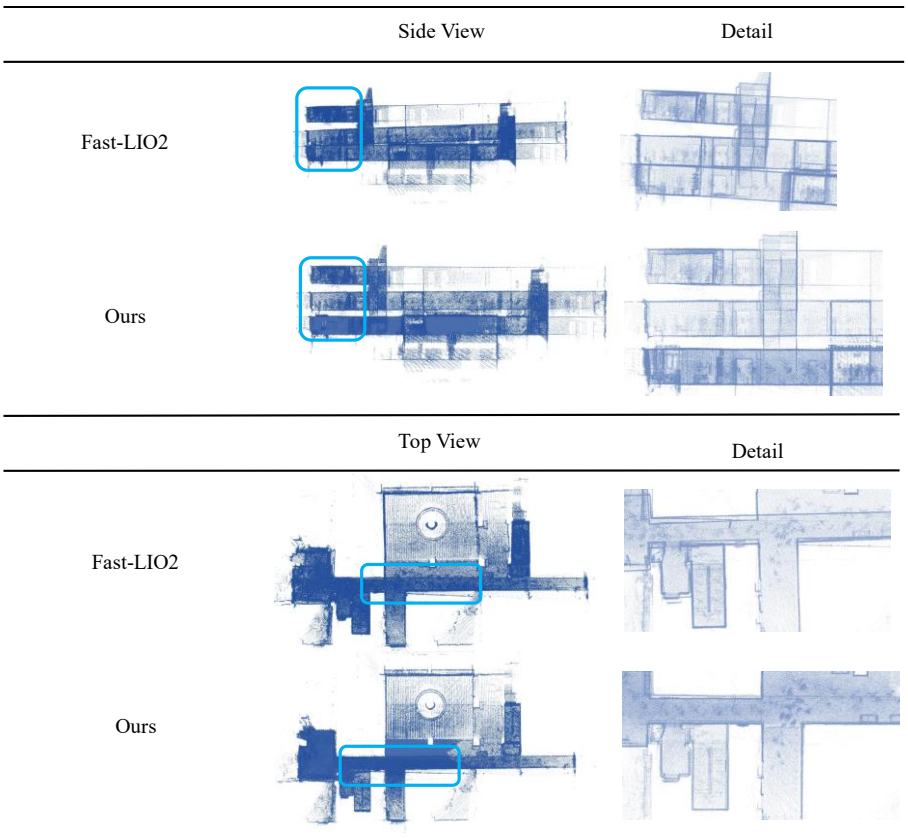

Figure 6. Multi-floor mapping results of different methods w\o rotating mechanism.

3.2 Comparative experiments

All of the experiments are conducted in a research lab building with typical wide and narrow multi-floor indoor hallways. In order to show the benefit brought by such rotating mechanism, we exam the mapping performance while turning on/off the motor. From each column of Figure 5, we can see many holes in the point cloud map when keeping the LiDAR still. Rotating can

obviously improve the efficiency of mapping tasks though with few improvements on the precision. In a word, the rotating framework not only improves the stability but also the efficiency of mapping system with larger coverage.

Moreover, comparative experiments are also executed on Fast-LIO2, a SOTA LIO method. As shown by each row of Figure 5, our method, whether rotating or not, achieves better performance compared to Fast-LIO2. The large distortions between the point cloud of different floors are rectified owing to the feature-based batch optimization. It can be clearly visualized from the top views and side views of Figure 6 that there are much more serious deviations in the point cloud map built by Fast-LIO2 not only in the height direction but horizontally. Although our method has obtained better global consistency, there are some slippages during the hall, caused by the LiDAR degeneracy in such environment.

4. Conclusions

In this paper, an effective multi-floor indoor mapping system is proposed incorporating the measurements from motor, IMU and LiDAR. Iterative ESKF is used for the LIO front-end, while a sliding-window-based optimization is conducted as the back-end. Linear/planar features are explicitly derived from the adaptive voxels to maintain the global consistency of point cloud map. Comparative experiments have shown the advantages of our mapping system. However, more datasets should be included in the future. What’s more, more attention is needed on the stability of batch optimization under degenerative scenes.

Acknowledgements

The paper is founded by Key Laboratory of Smart Earth (No. KF2023YB02-11) and State-funded postdoctoral researcher program (No. GZC20231482).

References

Alismail, H. and Browning, B., 2015. Automatic calibration of spinning actuated lidar internal parameters. *Journal of Field Robotics*, 32(5): 723-747.

Bosse, M., Zlot, R. and Flick, P., 2012. Zebedee: De-sign of a spring-mounted 3-d range sensor with application to mobile mapping. *IEEE Transactions on Robotics*, 28(5): 1104-1119.

Chen, K., Nemiroff, R. and Lopez, B.T., 2022. Direct LiDAR-Inertial Odometry. *arXiv preprint arXiv*:2203.03749.

Chen, K., Zhan, K., Pang, F., Yang, X. and Zhang, D., 2022. R-LIO: Rotating Lidar Inertial Odometry and Mapping. *Sustainability*, 14(17): 10833-10833.

Chen, P. et al., 2021. Low-drift odometry, mapping and ground segmentation using a backpack LiDAR system. *IEEE Robotics and Automation Letters*, 6(4): 7285-7292.

Claer, M., Ferrein, A. and Schiffer, S., 2019. Calibration of a rotating or revolving platform with a lidar sensor. *Applied Sciences*, 9(11): 2238-2238.

Duan, Y., Peng, J., Zhang, Y., Ji, J. and Zhang, Y., 2022. PFilter: Building Persistent Maps through Feature Filtering for Fast and Accurate LiDAR-based SLAM. *arXiv preprint arXiv*: 2208.14848.

Ebadi, K. et al., 2022. Present and Future of SLAM in Extreme Underground Environments. *arXiv preprint arXiv*:2208.01787.

Elhashash, M., Albanwan, H. and Qin, R., 2022. A Review of Mobile Mapping Systems: From Sensors to Applications. *arXiv preprint arXiv*:2205.15865.

Garcia-Fidalgo, E., Company-Corcoles, J.P., Bonnin-Pascual, F. and Ortiz, A., 2022. LiODOM: Adaptive local mapping for robust LiDAR-only odometry. *Robotics and Autonomous Systems*, 156: 104226-104226.

Holmberg, M., Karlsson, O. and Tulldahl, M., 2022. Lidar Positioning for Indoor Precision Navigation, *Proceedings of the IEEE/CVF Conference on Computer Vision and Pattern Recognition*, pp. 359-368.

Jiao, J., Ye, H., Zhu, Y. and Liu, M., 2021. Robust odometry and mapping for multi-lidar systems with online extrinsic calibration. *IEEE Transactions on Robotics*, 38(1): 351-371.

Kang, J. and Doh, N.L., 2016. Full-DOF calibration of a rotating 2-D LIDAR with a simple plane measurement. *IEEE Transactions on Robotics*, 32(5): 1245-1263.

Karimi, M., Oelsch, M., Stengel, O., Babaians, E. and Steinbach, E., 2021. LoLa-SLAM: low-latency LiDAR SLAM using continuous scan slicing. *IEEE Robotics and Automation Letters*, 6(2): 2248-2255.

Koide, K., Miura, J. and Menegatti, E., 2019. A portable three-dimensional LIDAR-based system for long-term and wide-area people behavior measurement. *International Journal of Advanced Robotic Systems*, 16(2): 1729881419841532

Le Gentil, C., Vidal-Calleja, T. and Huang, S., 2020. IN2LAAMA: Inertial lidar localization autocalibration and mapping. *IEEE Transactions on Robotics*. 37(1):275-90.

Lehtola, V.V. et al., 2022. Digital twin of a city: Re-view of technology serving city needs. *International Journal of Applied Earth Observation and Geoinformation*: 102915-102915.

Liu, X. et al., 2019. Optimized LOAM Using Ground Plane Constraints and SegMatch-Based Loop Detection. *Sensors*, 19(24): 5419-5419.

Liu, Z. and Zhang, F., 2021. Balm: Bundle adjustment for lidar mapping. *IEEE Robotics and Automation Letters*, 6(2): 3184-3191.

Morales, J. et al., 2018. Analysis of 3D scan measure-ment distribution with application to a multi-beam lidar on a rotating platform. *Sensors*, 18(2): 395-395.

Neumann, T., Dülberg, E., Schiffer, S. and Ferrein, A., 2016. A rotating platform for swift acquisition of dense 3D point clouds, *International Conference on Intelligent Robotics and Applications.* Springer, pp. 257-268.

Pan, Y., Xiao, P., He, Y., Shao, Z. and Li, Z., 2021. Mulls: Versatile LiDAR SLAM via Multi-metric Linear Least Square. *Proceedings - IEEE International Conference on Robotics and Automation*, 2021-May: 11633-11640.

Park, C. et al., 2021. Elasticity meets continuous-time: Map-centric dense 3D LiDAR SLAM. *IEEE Transactions on Robotics*, 38(2):978-97.

Qian, C., Xiang, Z., Wu, Z. and Sun, H., 2022. RF-LIO: Removal-First Tightly-coupled Lidar Inertial Odometry in High Dynamic Environments. *arXiv preprint arXiv*:2206.09463.

Quenzel, J. and Behnke, S., 2021. Real-time multi-adaptive-resolution-surfel 6D LiDAR odometry using continuous-time trajectory optimization, *2021 IEEE/RSJ International Conference on Intelligent Robots and Systems (IROS)*. IEEE, pp. 5499-5506.

Ramezani, M. et al., 2022. Wildcat: Online Continuous-Time 3D Lidar-Inertial SLAM. *arXiv preprint arXiv*:2205.12595.

Seo, D., Lim, H., Lee, S. and Myung, H., 2022. PaGO-LOAM: Robust Ground-Optimized LiDAR Odometry. *arXiv preprint arXiv*:2206.00266.

Shan, T. and Englot, B., 2018. Lego-loam: Lightweight and ground-optimized lidar odometry and mapping on variable terrain, *2018 IEEE/RSJ International Conference on Intelligent Robots and Systems (IROS)*. IEEE, pp. 4758-4765.

Velas, M., Spanel, M., Sleziak, T., Habrovec, J. and Herout, A., 2019. Indoor and outdoor backpack mapping with calibrated pair of velodyne LiDARs. *Sensors*, 19(18): 3944-3944.

Wang, Z., Yang, L., Gao, F. and Wang, L., 2022. FEVO-LOAM: Feature Extraction and Vertical Optimized Lidar Odometry and Mapping. *IEEE Robotics and Automation Letters*. 7(4):12086-93.

Wang, Z., Zhang, L., Shen, Y. and Zhou, Y., 2022. D-LIOM: Tightly-coupled Direct LiDAR-Inertial Odometry and Mapping. *IEEE Transactions on Multimedia*. 25:3905-20.

Wei, X., Lv, J., Sun, J. and Pu, S., 2021. Ground-SLAM: Ground Constrained LiDAR SLAM for Structured Multi-Floor Environments. *arXiv preprint arXiv*:2103.03713.

Xu, W. and Zhang, F., 2021. FAST-LIO: A Fast, Ro-bust LiDAR-Inertial Odometry Package by Tightly-Coupled Iterated Kalman Filter, *IEEE Robotics and Automation Letters*. 6(2):3317-24.

Yuan, C., Bi, S., Cheng, J., Yang, D. and Wang, W., 2021. Low-Cost Calibration of Matching Error between Lidar and Motor for a Rotating 2D Lidar. *Applied Sciences*, 11(3): 913-913.

Yuan, C., Xu, W., Liu, X., Hong, X. and Zhang, F., 2022. Efficient and probabilistic adaptive voxel map-ping for accurate online lidar odometry. *IEEE Robotics and Automation Letters*, 7(3): 8518-8525.

Zhang, J. and Singh, S., 2017. Low-drift and real-time lidar odometry and mapping. *Autonomous Robots*, 41(2): 401-416.

Zhen, W., Zeng, S. and Soberer, S., 2017. Robust localization and localizability estimation with a rotating laser scanner, *2017 IEEE international conference on robotics and automation (ICRA)*. IEEE, pp. 6240-6245.

Zhou, P., Guo, X., Pei, X. and Chen, C., 2021. T-LOAM: Truncated Least Squares LiDAR-Only Odometry and Mapping in Real Time. *IEEE Transactions on Geoscience and Remote Sensing*. 60:1-3.